



Cyclic Kite Configuration with Variable Mass of the Fifth Body in R5BP

¹Abdullah A. Ansari, ²Ashraf Ali, ³Mehtab Alam and ⁴Rabah Kellil

¹Department of Mathematics
College of Science Al-Zulfi
Majmaah University
Kingdom of Saudi Arabia
icairndin@gmail.com

²Department of Computer Science
College of Science Al-Zulfi
Majmaah University
Kingdom of Saudi Arabia
a.haidar@mu.edu.sa

³International Center for Advanced Interdisciplinary Research (ICAIR)
Ratiya Marg, Sangam Vihar
New Delhi, India
mehtab-alam@live.com

⁴Department of Mathematics
College of Science
Laghrour Abbes University Khenchela
Algeria
kellilrabah@yahoo.fr

Received: July 10, 2019; Accepted: November 11, 2019

Abstract

This paper presents a numerical investigation on some characteristics and parameters related to the motion of an infinitesimal body with variable mass in five-body problem. The other four bodies

are considered as primaries. The whole system forms a cyclic kite configuration and moves on a circle, the center of which is taken as the origin. We assume that the motion of the fifth infinitesimal body is affected by the other components of the system but it has no effect on their behavior. We started by setting the equations of motion of the fifth body by using Jeans' law and Meshcherskii's space-time transformations. Further, we determined numerically, using Mathematica software, the positions of Lagrangian points and basins of attraction in various planes. Finally, we investigated the linear stability of the Lagrangian points and noticed that all the Lagrangian points are unstable.

Keywords: Equilateral triangle; Variable mass; Zero-velocity curves; Basins of attraction

MSC 2010 No.: 70F15, 85A20, 70F05

1. Introduction

The restricted three-body and four-body problems, respectively denoted in the sequel by (R3BP) and (R4BP), attracted many researchers and are considered as important subjects of research in both celestial mechanics and astrophysics. Among the researchers that studied these problems, Jeans (1928) evaluated the binary system in the structure of the two-body problem with variable mass. Meshcherskii (1949) considered that the mass was emitted uniformly from the two-body system at high speeds towards the decay of the system. He also observed that there is change in orbits, angular momentum, and energy of the considered system. Abouelmagd et al. (2014) and Abouelmagd and Mostafa (2015) reviewed the perturbation effects on the R3BP and compressed the secular solution to the periodic solution. Abouelmagd and Ansari (2019) also studied the motion properties of the infinitesimal body in the framework of bi-circular Sun-perturbed Earth-Moon system with Jacobian integral, regions of motion, Poincaré surfaces of section and basins of attraction.

Ansari (2016(a), 2016(b), 2017(a), 2017(b), 2018), Ansari and Prasad (2018), Ansari and Alhusain (2019), and Ansari and Kellil (2019) revisited various restricted problems including three, four and five bodies with different perturbations as solar-radiation pressure, albedo-effect, different forms of the primaries (oblate, heterogeneous), and variation of mass etc. In their studies, they illustrated the graphs for equilibrium points, zero-velocity curves, Poincaré surfaces of section and basins of attraction and studied the stability of the stationary points and observed that in most cases, these stationary points are unstable. Kumari and Kushvah (2013) studied the effect of solar wind drag on the equilibrium points and zero-velocity curves in the restricted four-body problem. Marchesin et al. (2013) treated the spatial restricted rhomboidal Sitnikov's five-body problem and determined the Hamiltonian function and noticed that it has three degrees of independence depending periodically on time. In the same work, they characterized the regions of possible motion and shown that there are no chaos. Ollongren (1988), using the muMath package, studied the positions and stability of equilibrium points and generalized the study of classical restricted three-body problem to a particular restricted five-body problem.

Pandey and Ahmad (2013) investigated the motion of the infinitesimal body in the generalized frame of the Sitnikov problem. They considered that the four bodies, in which three are equal oblate

spheroids (the primaries), placed at the vertices of an equilateral triangle and moving in the circular orbits nearby their common center of mass and the infinitesimal body moving in the gravitational fields generated by the primaries in the z -direction and have no effect on the primaries. Ragos et al. (1997) investigated numerically the regions of quasi-periodic motion around non-symmetric periodic orbits in neighborhood of the triangular equilibrium points. They also observed that the regions studied surround in general the linearly stable segments of the corresponding families and become smaller as the mass ratio increases. Shahbaz and Hassan (2014) and Shahbaz et al. (2014) investigated the Sitnikov problem with cyclic kite configuration. They established the connection between three-body and four-body configurations of the problem, when the masses are close to zero. Shoaib et al. (2017) explored numerically and analytically the regions of possible motion on the planar central configuration of rhomboidal and triangular four-body and five-body problems.

Shrivastava and Ishwar (1983) determined equations of motion of the restricted three-body problem with decreasing mass, under the assumption that the mass of the infinitesimal body varies with respect to time. For the stability of equilibrium points in the restricted three-body problem with variable mass, we can cite Lukyanov (2009), where he noticed that for any set of parameters, all the stationary points in the problem are unstable with respect to the Meshcherskii's space-time transformations. Lichtenegger (1984) studied the dynamical behavior of the celestial bodies under the variable mass effect. Singh and Ishwar (1984, 1985, 2003, 2010 and 2016) studied various aspect of the effect of small perturbations in the coriolis and the centrifugal forces on the stability and location of stationary points, in the R3BP and R4BP. Zhang et al. (2012) studied the impact of solar radiation pressure on the R3BP with variable infinitesimal mass by using Jeans' law and Meshcherskii's space-time transformations.

As a contribution to the previously cited literature, we present in this paper the study of cyclic-kite-configuration in a restricted five-body problem, when the mass of the fifth body assumed infinitesimal, varies with time. The paper is organized as follows. In Section 2, we present and explain the model of our problem and determine the equation of motion. In Section 3, using Mathematica software, we draw the graphs for Lagrangian points and basins of attraction in various planes. The fourth section is devoted to the stability of the Lagrangian points. Finally, the fifth section represents a conclusion of our study.

2. Model of the problem and Equations of Motion

Assume that m_1, m_2, m_3, m_4 and $m(t)$ (with $m_1 = m_3$) are five masses, where $m_1, m_2, m_3,$ and m_4 will be the primaries, placed at the vertices of a cyclic kite $ABCD$ with radius R and move around a circle, center of which is taken as origin O . On the geometry of the kite, we introduce two restricted conditions: Firstly, ABC will be an equilateral triangle with $AB = BC = CA = \ell$ and secondly, ACD will be an isosceles triangle such that $AD = CD = R, AC = \ell,$ and $\ell = \sqrt{3}R$. The fifth variable mass $m(t)$ is moving under the gravitational forces $\vec{F}_1, \vec{F}_2, \vec{F}_3$ and \vec{F}_4 , exerted by $m_1, m_2, m_3,$ and m_4 respectively but its action on the primaries is supposed unimportant. Let $\vec{r}_1, \vec{r}_2, \vec{r}_3$ and \vec{r}_4 be the distances between the primaries, $m_1, m_2, m_3,$ and m_4 to the fifth body respectively. We also assume that m_1 is placed on the x -axis. Moreover, the coordinate axes are as

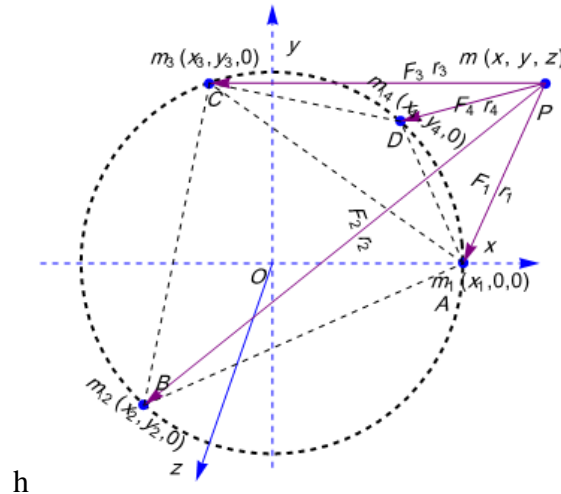


Figure 1. Cyclic kite configuration of the restricted five-body problem with infinitesimal variable mass.

clearly defined in Figure 1.

Let us consider the synodic coordinate system $(Oxyz)$ that coincides initially with the inertial coordinate system $(OXYZ)$, and revolving with angular velocity ω about the z -axis. In Figure 1 the five bodies m_1, m_2, m_3, m_4 and $m(t)$ are denoted by A, B, C, D and P respectively and their coordinates are $(x_1, 0, 0) = (R, 0, 0), (x_2, y_2, 0) = (-\frac{R}{2}, -\frac{\sqrt{3}R}{2}, 0), (x_3, y_3, 0) = (-\frac{R}{2}, \frac{\sqrt{3}R}{2}, 0), (x_4, y_4, 0) = (\frac{R}{2}, \frac{\sqrt{3}R}{2}, 0)$ and (x, y, z) , respectively.

Using a procedure similar to that used by Abouelmagd and Mostafa (2015), we got the following equations of motion of the fifth body in rotating coordinates system subjected to non-isotropic variation of mass with zero momentum resulting from one point,

$$\begin{cases} \frac{\dot{m}(t)}{m(t)}(\dot{x} - ny) + (\ddot{x} - 2n\dot{y}) = \Pi_x, \\ \frac{\dot{m}(t)}{m(t)}(\dot{y} + nx) + (\ddot{y} + 2n\dot{x}) = \Pi_y, \\ \frac{\dot{m}(t)}{m(t)}\dot{z} + \ddot{z} = \Pi_z, \end{cases} \quad (1)$$

where

$$\Pi = \frac{n^2}{2}(x^2 + y^2) + G \sum_{i=1}^4 \frac{m_i}{r_i}, \quad (2)$$

$\Pi_x, \Pi_y,$ and Π_z represent the partial derivatives of Π with respect to x, y and z , respectively, dot represents the differentiation with respect to time t and n is the mean motion which is also magnitude of the angular velocity ω .

For different dimensionless variables, we assume that,

$$\begin{aligned} R = 1, m_1 + m_2 + m_3 + m_4 = 1, G = 1, n = 1, m_2 = \mu, m_4 = \alpha_1\mu \\ \Rightarrow m_1 = m_3 = \frac{1 - \mu - \alpha_1\mu}{2}, \alpha_1 \ll 1. \end{aligned}$$

Hence, Equations (1) and (2) are reduced to

$$\begin{cases} \frac{\dot{m}(t)}{m(t)}(\dot{x} - y) + (\ddot{x} - 2\dot{y}) = W_x, \\ \frac{\dot{m}(t)}{m(t)}(\dot{y} + x) + (\ddot{y} + 2\dot{x}) = W_y, \\ \frac{\dot{m}(t)}{m(t)}\dot{z} + \ddot{z} = W_z, \end{cases} \tag{3}$$

where

$$\begin{cases} W = \frac{1}{2}(x^2 + y^2) + \frac{1-\mu-\alpha_1\mu}{2r_1} + \frac{\mu}{r_2} + \frac{1-\mu-\alpha_1\mu}{2r_3} + \frac{\alpha_1\mu}{r_4}, \\ r_i^2 = (x - x_i)^2 + (y - y_i)^2 + z^2, i = 1, 2, 3, 4. \end{cases} \tag{4}$$

Due to variation of mass of the fifth body, using Jeans' law and Meshcherskii's space-time transformations, the above equations can be simplified as

$$\frac{dm(t)}{dt} = -\lambda_1 m(t), \quad \alpha = \epsilon^{\frac{1}{2}}x, \beta = \epsilon^{\frac{1}{2}}y, \gamma = \epsilon^{\frac{1}{2}}z, d\tau = dt, \rho_i = \epsilon^{\frac{1}{2}}r_i, (i = 1, 2),$$

where $\epsilon = \frac{m(t)}{m_0}$, (it is clear that ϵ is less than unity when the mass decreases and greater than unity when the mass increases respectively to m_0 , the initial mass of the fifth body) and λ_1 is a variation parameter which is constant. We got

$$\begin{cases} \frac{d\epsilon}{dt} = -\lambda_1\epsilon, \\ \dot{x} = \epsilon^{-1/2}(\alpha' + \frac{\lambda_1}{2}\alpha), \quad \ddot{x} = \epsilon^{-1/2}(\alpha'' + \lambda_1\alpha' + \frac{\lambda_1^2}{4}\alpha), \\ \dot{y} = \epsilon^{-1/2}(\beta' + \frac{\lambda_1}{2}\beta), \quad \ddot{y} = \epsilon^{-1/2}(\beta'' + \lambda_1\beta' + \frac{\lambda_1^2}{4}\beta), \\ \dot{z} = \epsilon^{-1/2}(\gamma' + \frac{\lambda_1}{2}\gamma), \quad \ddot{z} = \epsilon^{-1/2}(\gamma'' + \lambda_1\gamma' + \frac{\lambda_1^2}{4}\gamma), \end{cases} \tag{5}$$

where (') denotes the differentiation with respect to τ .

Finally, the equations of motion become

$$\begin{cases} \ddot{\alpha} - 2\dot{\beta} = \Psi_\alpha, \\ \ddot{\beta} + 2\dot{\alpha} = \Psi_\beta, \\ \ddot{\gamma} = \Psi_\gamma, \end{cases} \tag{6}$$

where

$$\begin{cases} \Psi = \frac{1}{2}(\alpha^2 + \beta^2) + \frac{\lambda_1^2}{8}(\alpha^2 + \beta^2 + \gamma^2) + \epsilon^{3/2}\left\{\frac{1-\mu-\alpha_1\mu}{2\rho_1} + \frac{\mu}{\rho_2} + \frac{1-\mu-\alpha_1\mu}{2\rho_3} + \frac{\alpha_1\mu}{\rho_4}\right\}, \\ \rho_i^2 = (\alpha - x_i\epsilon^{1/2})^2 + (\beta - y_i\epsilon^{1/2})^2 + \gamma^2, \quad i = 1, 2, 3, 4. \end{cases} \tag{7}$$

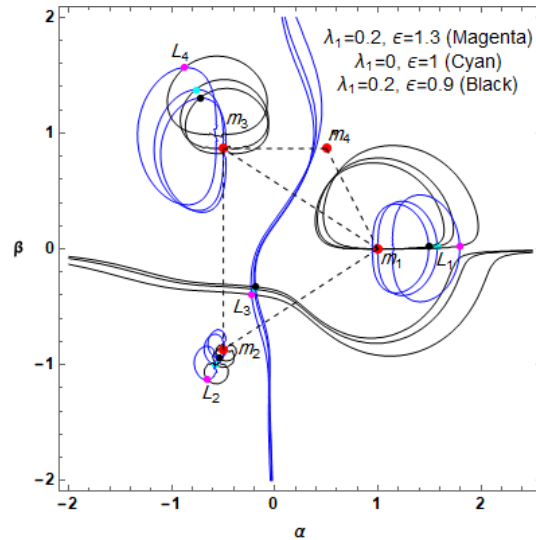


Figure 2. Positions of Lagrangian points in $\alpha - \beta$ - plane. Where red colors denote the positions of the primaries

3. Numerical Analysis

In this section, from our data we have drawn Lagrangian points and basins of attraction in various planes. These graphs reveal the dynamical behavior of the infinitesimal body. In all our numerical calculations, we took $\mu = 0.019$, $\alpha_1 = 0.01$ and $\lambda_1 = 0.2$.

3.1. Lagrangian points

The Lagrangian points can be determined by solving the equations

$$\frac{\partial \Psi}{\partial \alpha} = 0, \quad \frac{\partial \Psi}{\partial \beta} = 0 \quad \text{and} \quad \frac{\partial \Psi}{\partial \gamma} = 0,$$

in the following two different planes:

- In-plane motion ($\alpha, \beta, \gamma = 0$),
- Out-of planes motion ($(\alpha, \beta = 0, \gamma)$ and $(\alpha = 0, \beta, \gamma)$).

3.1.1. In-plane motion

In this subsection, we have plotted the locations of Lagrangian points in (α, β) -plane (Figure 2), for the values $\epsilon = 1.3$, $\epsilon = 1$ and $\epsilon = 0.9$. We found four Lagrangian points that we have denoted by L_1 , L_2 , L_3 and L_4 . One, say (L_1) is on the α -axis and the others Lagrangian points L_2 , L_3 , L_4 are non-collinear. All the Lagrangian points are located near the primaries. More precisely, L_1 is located near m_1 , L_2 and L_3 are located near m_2 and L_4 is located near m_3 . However, there is no Lagrangian point located near the primary m_4 . Furthermore, from the figure, we observed that L_1

is moving towards m_1 , L_2 is moving towards m_2 while L_3 is moving away from m_2 and L_4 is moving towards m_3 , as the value of ϵ decreases. So, the variation of ϵ produces a great impact on the Lagrangian points during in-plane motion.

3.1.2. Out-of-plane motion

During the out-of-plane ($\alpha, \beta = 0, \gamma$), we found at most four Lagrangian points (L_1, L_2, L_3, L_4). L_1 and L_2 are located on α -axis, while L_3 and L_4 are located on γ -axis (Figure 3).

On the other hand, during the out-of-plane ($\alpha = 0, \beta, \gamma$), we found at most three Lagrangian points (L_1, L_2, L_3) in which L_1 is on β -axis, located near the origin and (L_2, L_3) are on γ -axis (Figure 4). It is easy to see that, the variation constant ϵ has also in this situation a qualitative impact on the location of Lagrangian points.

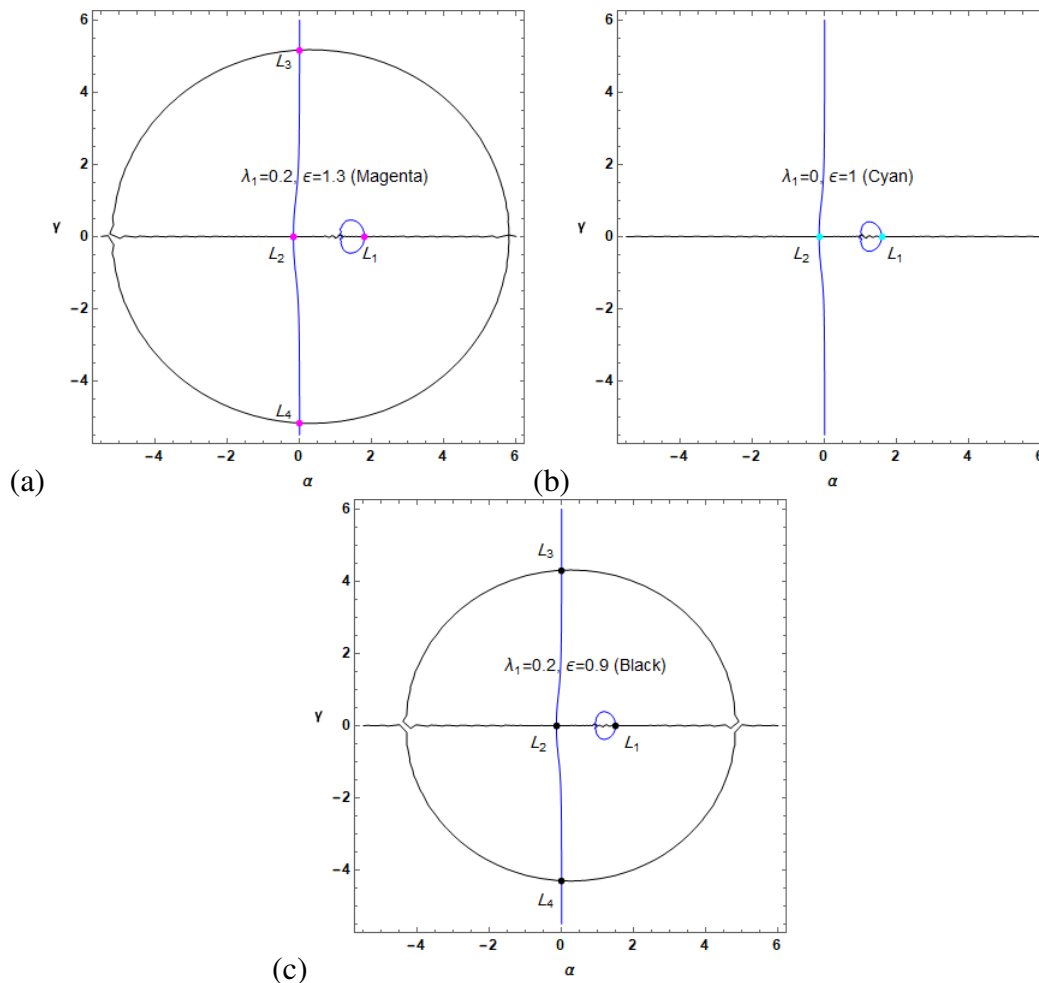


Figure 3. Positions of Lagrangian points in $\alpha - \gamma$ plane at $\epsilon = 1.3(a), 1(b), 0.9(c)$

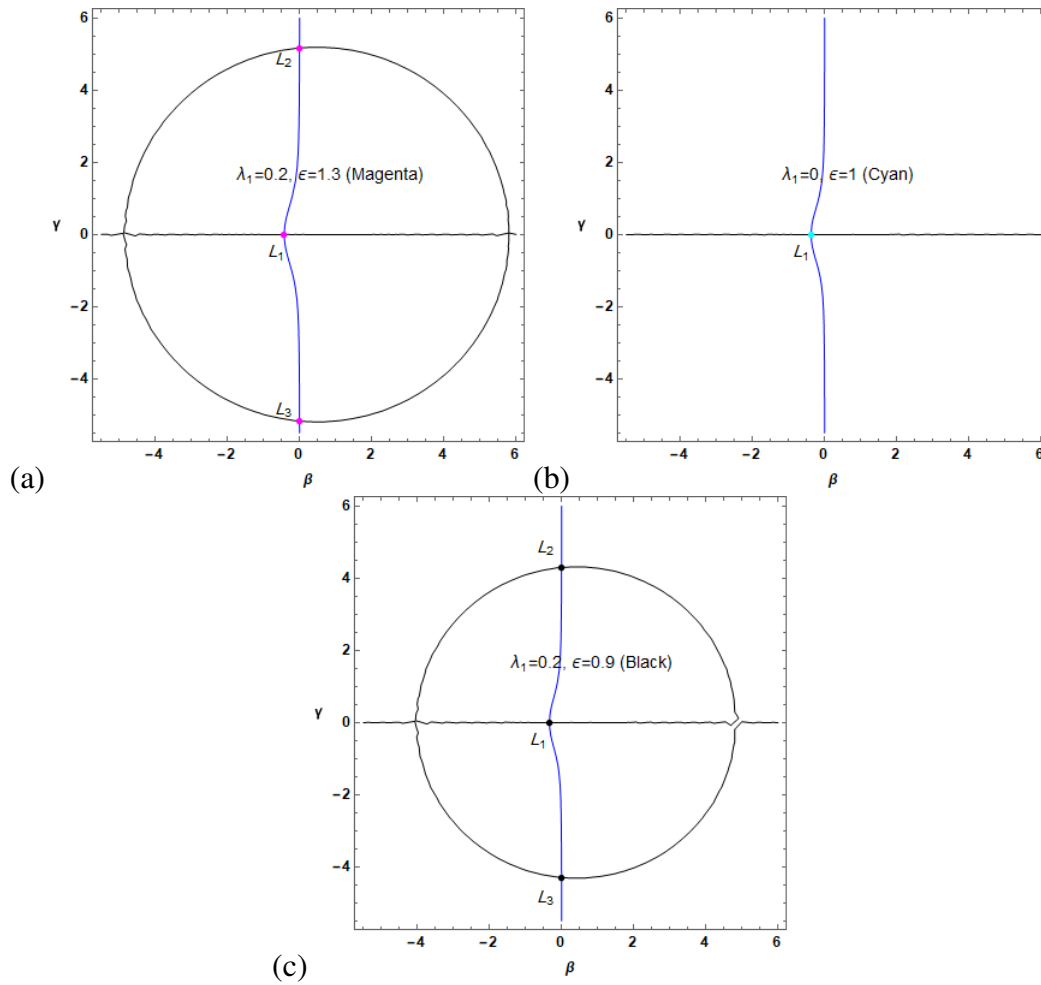


Figure 4. Positions of Lagrangian points in $\beta - \gamma$ - plane at $\epsilon = 1.3(a), 1(b), 0.9(c)$

3.2. Basins of attraction

By using simple, fast and accurate N-R iterative method to solve the multivariate functions, we have drawn in this subsection, the basins of attraction for our cyclic kite configuration. The regions of convergence are composed by all the initial values that tend to a specific Lagrangian points. The basins of convergence is one of the most important qualitative properties of the dynamical systems. It is illustrated by following procedure: After classifying dense uniform grid of 1024×1024 initial conditions, multiple scan of the configuration plane is done. By considering the maximum number of iterations as 500, we set the predefined accuracy as 10^{-15} . Using the cited above iterative method, we plotted the basins of convergence in three planes; (α, β) -plane (Figure 6a), (α, γ) -plane (Figure 7a) and (β, γ) -plane (Figure 7b)). The algorithm of our problem in (α, β) -plane when $\gamma = 0$, is represented by the following iterative process:

$$\alpha_{n+1} = \alpha_n - \left(\frac{\Psi_\alpha \Psi_{\beta\beta} - \Psi_\beta \Psi_{\alpha\beta}}{\Psi_{\alpha\alpha} \Psi_{\beta\beta} - \Psi_{\alpha\beta} \Psi_{\beta\alpha}} \right)_{(\alpha_n, \beta_n)}, \tag{8}$$

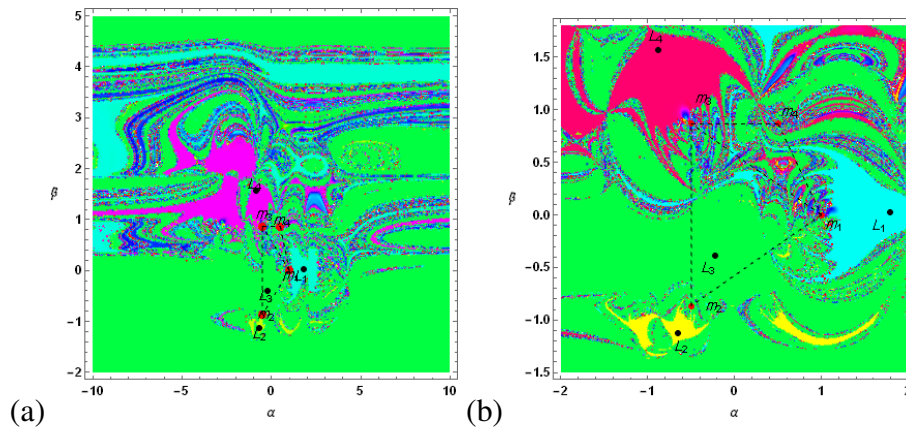


Figure 5. (a) Basins of Convergence with cyclic kite configuration of the primaries in $\alpha - \beta$ - plane at $\epsilon = 1.3$
 (b) Zoomed part of (a) near the cyclic kite configuration

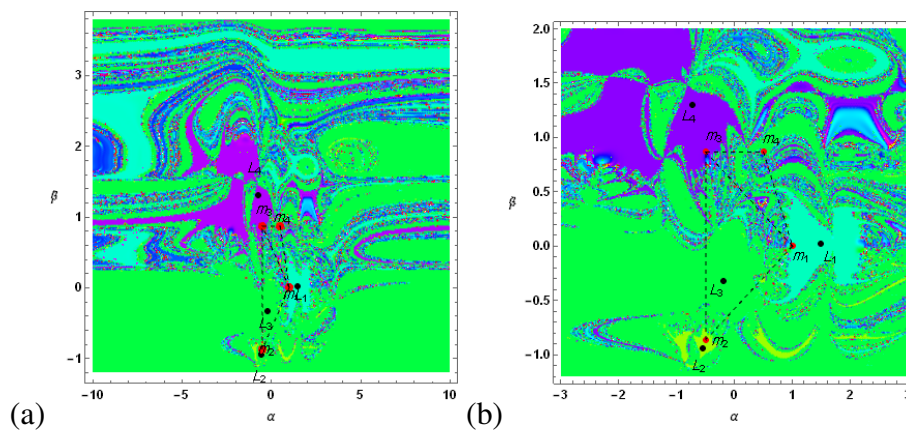


Figure 6. (a) Basins of Convergence with cyclic kite configuration of the primaries in $\alpha - \beta$ - plane at $\epsilon = 0.9$
 (b) Zoomed part of (a) near the cyclic kite configuration

$$\beta_{n+1} = \beta_n - \left(\frac{\Psi_\beta \Psi_{\alpha\alpha} - \Psi_\alpha \Psi_{\beta\alpha}}{\Psi_{\alpha\alpha} \Psi_{\beta\beta} - \Psi_{\alpha\beta} \Psi_{\beta\alpha}} \right)_{(\alpha_n, \beta_n)}, \tag{9}$$

where α_n, β_n are the values of α and β coordinates of the n^{th} step of the N-R iterative process. If the initial point converges rapidly to one of the Lagrangian points then this point (α, β) will be a member of the basin of convergence. This process stops when the successive approximation converges to a Lagrangian point. For the classification of different Lagrangian points on the planes, we used a color code.

In (α, β) -plane, we have drawn the basins of convergence for $\epsilon = 1.3$ (Figure 5a) and for $\epsilon = 0.9$ (Figure 6a). We observed that there are four attracting points $L_1, L_2, L_3,$ and L_4 in both these figures. From Figure 5a, we found that L_1 corresponds to the cyan color region, L_2 corresponds to the yellow color region, L_3 corresponds to the green color region and L_4 corresponds to the magenta color region. And from Figure 6a, we found the same color regions for $L_1, L_2,$ and L_3 but for L_4 purple color region. And we also observed that L_1 and L_2 have finite color regions but L_3 and L_4 extend to the infinite color regions.

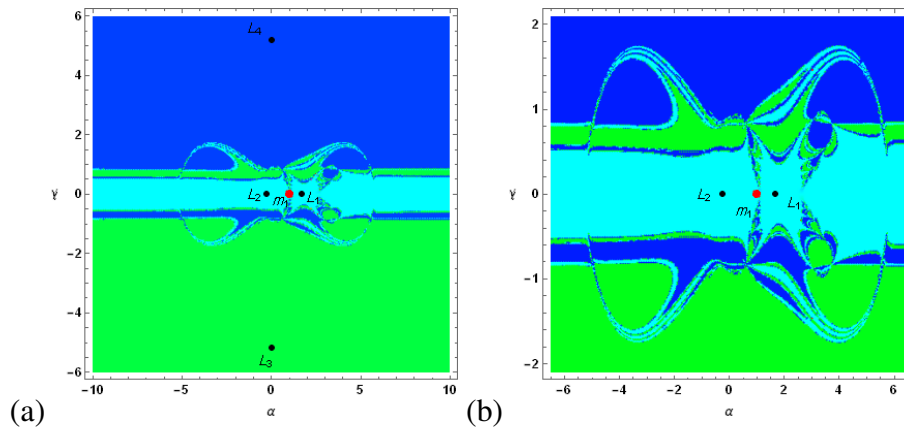


Figure 7. (a) Basins of Convergence with cyclic kite configuration of the primaries in $\alpha - \gamma$ - plane at $\epsilon = 1.3$
 (b) Zoomed part of (a) near the cyclic kite configuration

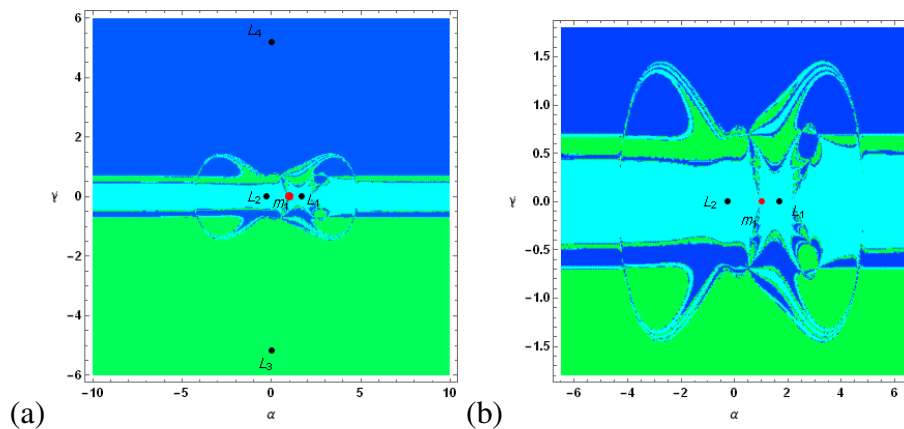


Figure 8. (a) Basins of Convergence with cyclic kite configuration of the primaries in $\alpha - \gamma$ - plane at $\epsilon = 0.9$
 (b) Zoomed part of (a) near the cyclic kite configuration

Similarly, we easily determined the algorithm for the other two (α, γ) -plane (Figures 7a, 8a), and (β, γ) -plane (Figures 9a, 10a).

In (α, γ) -plane, we found four attracting points L_1 , L_2 , L_3 , and L_4 . L_1 and L_2 represented by, cyan color regions, while L_3 and L_4 by green and blue color regions respectively. Moreover, all the color regions extend to infinity.

In (β, γ) -plane, we found the same phenomenon as in (α, γ) -plane for three attracting points L_1 , L_2 , and L_3 . In the figures, L_1 , L_2 and L_3 were represented by, cyan, green and blue color regions respectively. Furthermore, all the color regions extend to infinity.

We observed, when we reduced the values of the variation constant ϵ , that the corresponding curves are shrinking in all the studied planes. Notice that, in all the figures related to this subsection, red points represent the positions of the primaries.

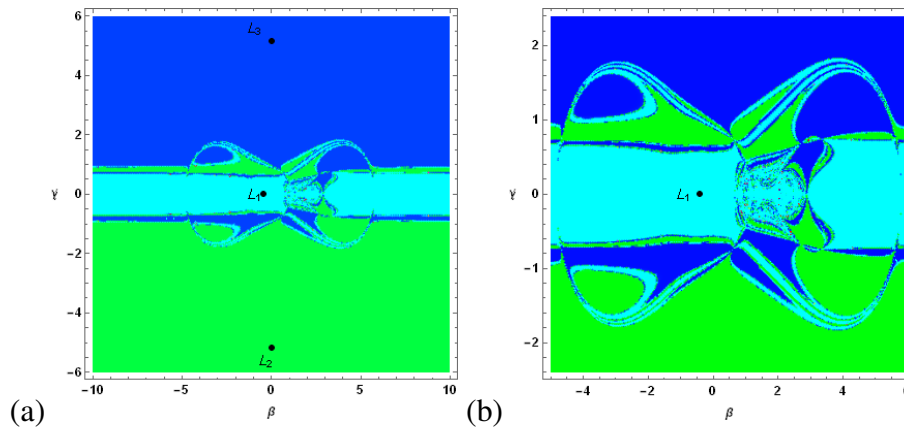


Figure 9. (a) Basins of Convergence with cyclic kite configuration of the primaries in $\beta - \gamma$ - plane at $\epsilon = 1.3$
 (b) Zoomed part of (a) near the cyclic kite configuration

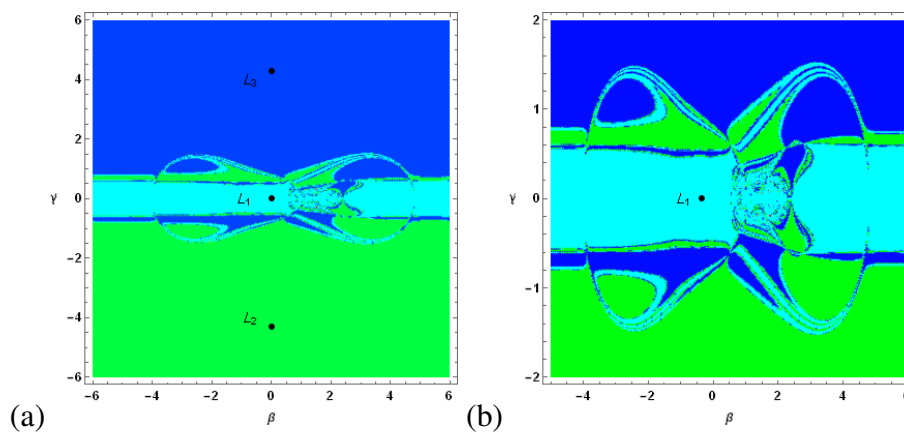


Figure 10. (a) Basins of Convergence with cyclic kite configuration of the primaries in $\beta - \gamma$ - plane at $\epsilon = 0.9$
 (b) Zoomed part of (a) near the cyclic kite configuration

4. Linear stability of Lagrangian points

This section is devoted to the stability of Lagrangian points by giving the displacements $((u, v, w) \ll 1)$ to $(\alpha_0, \beta_0, \gamma_0)$ as

$$\begin{cases} \alpha = u + \alpha_0, \\ \beta = v + \beta_0, \\ \gamma = w + \gamma_0, \end{cases} \tag{10}$$

where $(\alpha_0, \beta_0, \gamma_0)$ is the Lagrangian point that corresponds to a fixed value of time t_0 . The variational equations deduced from the equations (6) and (10) can be written as follows:

$$\begin{cases} \ddot{u} - 2\dot{v} = (\Psi_{\alpha\alpha})_0 u + (\Psi_{\alpha\beta})_0 v + (\Psi_{\alpha\gamma})_0 w, \\ \ddot{v} + 2\dot{u} = (\Psi_{\beta\alpha})_0 u + (\Psi_{\beta\beta})_0 v + (\Psi_{\beta\gamma})_0 w, \\ \ddot{w} = (\Psi_{\gamma\alpha})_0 u + (\Psi_{\gamma\beta})_0 v + (\Psi_{\gamma\gamma})_0 w. \end{cases} \tag{11}$$

In the phase-plane, system (11) can be expressed as

$$\begin{cases} \dot{u} = u_1, \\ \dot{v} = v_1, \\ \dot{w} = w_1, \\ \dot{u}_1 = (\Psi_{\alpha\alpha})_0 u + (\Psi_{\alpha\beta})_0 v + (\Psi_{\alpha\gamma})_0 w + 2v_1, \\ \dot{v}_1 = (\Psi_{\beta\alpha})_0 u + (\Psi_{\beta\beta})_0 v + (\Psi_{\beta\gamma})_0 w - 2u_1, \\ \dot{w}_1 = (\Psi_{\gamma\alpha})_0 u + (\Psi_{\gamma\beta})_0 v + (\Psi_{\gamma\gamma})_0 w. \end{cases} \tag{12}$$

Due to the variation of distances between primaries and the Lagrangian points $(\alpha_0, \beta_0, \gamma_0)$, methods usually used to study stability were inadequate. We therefore used the following Meshcherskii' space-time inverse transformations

$$x' = \epsilon^{-1/2}u, y' = \epsilon^{-1/2}v, z' = \epsilon^{-1/2}w, u' = \epsilon^{-1/2}u_1, v' = \epsilon^{-1/2}v_1, w' = \epsilon^{-1/2}w_1.$$

These transformations reduced the previous equations to the following, expressed in the matrix form as

$$\begin{pmatrix} \frac{dx'}{dt} \\ \frac{dy'}{dt} \\ \frac{dz'}{dt} \\ \frac{du'}{dt} \\ \frac{dv'}{dt} \\ \frac{dw'}{dt} \end{pmatrix} = A \times \begin{pmatrix} x' \\ y' \\ z' \\ u' \\ v' \\ w' \end{pmatrix}, \tag{13}$$

where

$$A = \begin{pmatrix} \frac{\lambda_1}{2} & 0 & 0 & 1 & 0 & 0 \\ 0 & \frac{\lambda_1}{2} & 0 & 0 & 1 & 0 \\ 0 & 0 & \frac{\lambda_1}{2} & 0 & 0 & 1 \\ (\Psi_{\alpha\alpha})_0 & (\Psi_{\alpha\beta})_0 & (\Psi_{\alpha\gamma})_0 & \frac{\lambda_1}{2} & 2 & 0 \\ (\Psi_{\beta\alpha})_0 & (\Psi_{\beta\beta})_0 & (\Psi_{\beta\gamma})_0 & -2 & \frac{\lambda_1}{2} & 0 \\ (\Psi_{\gamma\alpha})_0 & (\Psi_{\gamma\beta})_0 & (\Psi_{\gamma\gamma})_0 & 0 & 0 & \frac{\lambda_1}{2} \end{pmatrix}.$$

Due to the invariance of the distances from the primaries to the Lagrangian points, the linear stability of (6) and (13) should be consistent. Thus, the linear stability of this solution depends on the existence of stable region of the Lagrangian point, which in turn depends on the boundedness of the solution of a linear homogenous system of Equation (13).

And hence, we deduced the characteristic equation of the matrix A as

$$\lambda^6 + a_5\lambda^5 + a_4\lambda^4 + a_3\lambda^3 + a_2\lambda^2 + a_1\lambda + a_0 = 0, \tag{14}$$

where

$$\begin{aligned}
 a_5 &= -3\lambda_1, \\
 a_4 &= 4 - \Psi_{\alpha\alpha} - \Psi_{\beta\beta} - \Psi_{\gamma\gamma} + \frac{15}{4}\lambda_1^2, \\
 a_3 &= 2(-4 + \Psi_{\alpha\alpha} + \Psi_{\beta\beta} + \Psi_{\gamma\gamma})\lambda_1 - \frac{5}{2}\lambda_1^3, \\
 a_2 &= -\Psi_{\alpha\beta}^2 - \Psi_{\alpha\gamma}^2 + \Psi_{\alpha\alpha}\Psi_{\beta\beta} - \Psi_{\beta\gamma}^2 - 4\Psi_{\gamma\gamma} \\
 &\quad + \Psi_{\alpha\alpha}\Psi_{\gamma\gamma} + \Psi_{\beta\beta}\Psi_{\gamma\gamma} - \frac{3}{2}(-4 + \Psi_{\alpha\alpha} + \Psi_{\beta\beta} + \Psi_{\gamma\gamma})\lambda_1^2 + \frac{15\lambda_1^4}{16}, \\
 a_1 &= (\Psi_{\alpha\beta}^2 + \Psi_{\alpha\gamma}^2 - \Psi_{\alpha\alpha}\Psi_{\beta\beta} + \Psi_{\beta\gamma}^2 - (-4 + \Psi_{\alpha\alpha} + \Psi_{\beta\beta})\Psi_{\gamma\gamma})\lambda_1 \\
 &\quad + \frac{1}{2}(-4 + \Psi_{\alpha\alpha} + \Psi_{\beta\beta} + \Psi_{\gamma\gamma})\lambda_1^3 - \frac{3}{16}\lambda_1^5, \\
 a_0 &= \frac{\lambda_1^6}{64} - \frac{\lambda_1^4}{16}(-4 + \Psi_{\alpha\alpha} + \Psi_{\beta\beta} + \Psi_{\gamma\gamma}) - \frac{\lambda_1^2}{4}(\Psi_{\alpha\beta}^2 + \Psi_{\alpha\gamma}^2 - \Psi_{\alpha\alpha}\Psi_{\beta\beta} + \Psi_{\beta\gamma}^2 \\
 &\quad - (-4 + \Psi_{\alpha\alpha} + \Psi_{\beta\beta})\Psi_{\gamma\gamma}) + \Psi_{\alpha\gamma}^2\Psi_{\beta\beta} - 2\Psi_{\alpha\beta}\Psi_{\alpha\gamma}\Psi_{\beta\gamma} + \Psi_{\alpha\beta}^2\Psi_{\gamma\gamma} + \Psi_{\alpha\alpha}(\Psi_{\beta\gamma}^2 - \Psi_{\beta\beta}\Psi_{\gamma\gamma}).
 \end{aligned}$$

The roots (called in the sequel characteristic roots) of the above equation have been calculated in three planes and for various values of the mass parameter ϵ (see Tables 1 – 6). We observed from the tables the existence of at least one positive real root (dark black in tables) or having a positive real part corresponding to each Lagrangian points. Therefore, all the Lagrangian points either in-plane or out-of-planes are unstable.

5. Conclusion

We studied the effect of the variation of mass parameter ϵ of the infinitesimal body in the restricted five-body problem having cyclic kite configuration. We found that the variation of this parameter ϵ has a great impact on the Lagrangian points, basins of attraction and on the stability of the Lagrangian points. Due to the variation of this parameter, our equations of motion are different from those characterizing the classical case by the parameters λ_1 and ϵ . As we decreased the value of ϵ , we observed that the Lagrangian points are moving towards the origin. Moreover, for the basins of attraction, we found that they are shrinking. Finally, from the data recorded in Tables 1-6, we concluded that all the Lagrangian points are unstable.

Table 1. Characteristic roots and their nature of stability for each Lagrangian points at $\mu = 0.019$, $\alpha_1 = 0.1$, $\lambda_1 = 0.2$, $\epsilon = 1.3$ in $\alpha - \beta$ -plane

No.	Lagrangian points (α, β)	Corresponding Characteristic roots ($\lambda_1, \lambda_2, \lambda_3, \lambda_4, \lambda_5, \lambda_6$)	Nature
1	-0.6526803875, -1.1304755924	0.0999999999 \pm 2.5670651738 i, 0.1000000000 \pm 2.5280212457 i, 3.4182397481 , -3.2182397481	Unstable
2	1.7927222166, 0.0253181224	0.0999999999 \pm 1.6961750281 i, 0.1000000000 \pm 1.6265290970 i, 1.9848359689 , -1.7848359689	Unstable
3	-0.8744349710, 1.5652020427	0.0999999999 \pm 1.6265290970 i, 0.1000000000 \pm 1.6961750281 i, 1.9848359689 , -1.7848359689	Unstable
4	-0.2266201602, -0.3925176315	-0.4490762472 \pm 0.9976146600 i, 0.0999999999 \pm 0.7632165030 i, 0.6490762472 \pm 0.9976146600 i,	Unstable

Table 2. Characteristic roots and their nature of stability for each Lagrangian points at $\mu = 0.019$, $\alpha_1 = 0.1$, $\lambda_1 = 0.2$, $\epsilon = 0.9$ in $\alpha - \beta$ -plane

No.	Lagrangian points (α, β)	Corresponding Characteristic roots ($\lambda_1, \lambda_2, \lambda_3, \lambda_4, \lambda_5, \lambda_6$)	Nature
1	-0.5430657660, -0.9406174986	0.0999999999 \pm 2.5669125092 i, 0.1000000000 \pm 2.5278668397 i, 3.4180040068 , -3.2180040068	Unstable
2	1.4916350480, 0.0210659512	0.0999999999 \pm 1.6265290970 i, 0.1000000000 \pm 1.6961750281 i, 1.9848359689 , -1.7848359689	Unstable
3	-0.7275738750, 1.3023268203	0.0999999999 \pm 1.6265290970 i, 0.1000000000 \pm 1.6961750281 i, 1.9848359689 , -1.7848359689	Unstable
4	-0.1884963043, -0.3264851761	-0.4491137791 \pm 0.9976205608 i, 0.1000000000 \pm 0.7632550807 i, 0.6491137791 \pm 0.9976205608 i,	Unstable

Table 3. Characteristic roots and their nature of stability for each Lagrangian points at $\mu = 0.019, \alpha_1 = 0.1, \lambda_1 = 0.2, \epsilon = 1.3$ in $\alpha - \gamma$ -plane

No.	Lagrangian points (α, β)	Corresponding Characteristic roots ($\lambda_1, \lambda_2, \lambda_3, \lambda_4, \lambda_5, \lambda_6$)	Nature
1	-0.0020627558, -5.1821717268	0.0723888473 \pm 0.9999958748 i, 0.1276111526 \pm 0.9999958748 i, 0.2686972074 , -0.0686972074	Unstable
2	-0.0020627558, 5.1821717268	0.0723888473 \pm 0.9999958748 i, 0.1276111526 \pm 0.9999958748 i, 0.2686972074 , -0.0686972074	Unstable
3	1.6781872907, 0.0000000000	0.0999999999 \pm 2.1699514381 i, 0.1000000000 \pm 2.2308597011 i, 2.8776652516 , -2.6776652516	Unstable
4	-0.2472617685, 0.0000000000	-0.5315273567 \pm 0.9570503970 i, 0.0999999999 \pm 0.9673482720 i, 0.7315273567 \pm 0.9570503970 i,	Unstable

Table 4. Characteristic roots and their nature of stability for each Lagrangian points at $\mu = 0.019, \alpha_1 = 0.1, \lambda_1 = 0.2, \epsilon = 0.9$ in $\alpha - \gamma$ -plane

No.	Lagrangian points (α, β)	Corresponding Characteristic roots ($\lambda_1, \lambda_2, \lambda_3, \lambda_4, \lambda_5, \lambda_6$)	Nature
1	-0.0022342685, 4.2993018357	0.0999999999 \pm 0.9278855224 i, 0.1000000000 \pm 1.0720816689 i, 0.3008249180 , -0.1008249180	Unstable
2	-0.0022342685, -4.2993018357	0.0999999999 \pm 1.0720816689 i, 0.1000000000 \pm 0.9278855224 i, 0.3008249180 , -0.1008249180	Unstable
3	1.4919710745, 0.0000000000	0.0999999999 \pm 4.1274407531 i, 0.1000000000 \pm 4.0925249867 i, 5.7404368570 , -5.5404368570	Unstable
4	-0.1426340457, 0.0000000000	-0.5457439910 \pm 0.9652293089 i, 0.1000000000 \pm 0.9698635813 i, 0.7457439910 \pm 0.9652293089 i,	Unstable

Table 5. Characteristic roots and their nature of stability for each Lagrangian points at $\mu = 0.019$, $\alpha_1 = 0.1$, $\lambda_1 = 0.2$, $\epsilon = 1.3$ in $\beta - \gamma$ -plane

No.	Lagrangian points (α, β)	Corresponding Characteristic roots ($\lambda_1, \lambda_2, \lambda_3, \lambda_4, \lambda_5, \lambda_6$)	Nature
1	-0.0046552311, -5.1675230862	0.0736526666 \pm 0.9999957424 i, 0.1263473333 \pm 0.9999957424 i, 0.2690993970 , -0.0690993970	Unstable
2	-0.0046552311, 5.1675230862	0.0736526666 \pm 0.9999957424 i, 0.1263473333 \pm 0.9999957424 i, 0.2690993970 , -0.0690993970	Unstable
3	-0.4268478186, 0.0000000000	-0.4635081962 \pm 0.9879433393 i, 0.0999999999 \pm 0.8080958427 i, 0.6635081962 \pm 0.9879433393 i,	Unstable

Table 6. Characteristic roots and their nature of stability for each Lagrangian points at $\mu = 0.019$, $\alpha_1 = 0.1$, $\lambda_1 = 0.2$, $\epsilon = 0.9$ in $\beta - \gamma$ -plane

No.	Lagrangian points (α, β)	Corresponding Characteristic roots ($\lambda_1, \lambda_2, \lambda_3, \lambda_4, \lambda_5, \lambda_6$)	Nature
1	-0.0038880775, -4.2939476570	0.0742974156 \pm 0.9999956998 i, 0.1257025843 \pm 0.9999956998 i, 0.2692972345 , -0.0692972345	Unstable
2	-0.0038880775, -4.2939476570	0.0742974156 \pm 0.9999956998 i, 0.1257025843 \pm 0.9999956998 i, 0.2692972345 , -0.0692972345	Unstable
3	-0.3386262196, 0.0000000000	-0.4697483286 \pm 0.9885728388 i, 0.0999999999 \pm 0.8152752914 i, 0.6697483286 \pm 0.9885728388 i,	Unstable

Acknowledgment:

The authors are presenting their thanks to the anonymous referees for giving their valuable suggestions to reach up to the present form of this manuscript.

REFERENCES

- Abouelmagd, E.I. and Ansari, A.A. (2019). The motion properties of the infinitesimal body in the framework of bicircular Sun-perturbed Earth-Moon system, *New Astronomy*, Vol. 73, No. 101282. <https://doi.org/10.1016/j.newast.2019.101282>
- Abouelmagd, E.I., Awad, M.E., Elzayat, E.M.A. and Abbas, I.A. (2014). Reduction the secular solution to periodic solution in the generalized restricted three-body problem, *Astrophysics and Space Science*, Vol. 350, No. 2, pp. 495-505.
- Abouelmagd, E.I. and Mostafa, A. (2015). Out of plane equilibrium points locations and the forbidden movement regions in the restricted three-body problem with variable mass, *Astrophys. Space Sci.*, Vol. 357, No. 58. doi:10.1007/s10509-015-2294-7
- Ansari, A.A. (2016(a)). The photogravitational circular restricted four-body problem with variable masses, *Journal of Engineering and Applied Sciences*, Vol. 3, No. 2, pp. 30-38.
- Ansari, A.A. (2016(b)). Stability of the equilibrium points in the circular restricted four-body problem with oblate primary and variable mass, *International Journal of Advanced Astronomy*, Vol. 4, No. 1, pp. 14-19.
- Ansari, A.A. (2017(a)). The circular restricted four-body problem with variable masses, *Nonlinear Sci. Lett. A*, Vol. 8, No. 3, pp. 303-312.
- Ansari, A.A. (2017(b)). Effect of Albedo on the motion of the infinitesimal body in circular restricted three-body problem with variable masses, *Italian J. of Pure and Applied Mathematics*, Vol. 38, pp. 581-600.
- Ansari, A.A. (2018). The circular restricted four-body problem with triaxial primaries and variable mass, *Applications and Applied Mathematics: An International Journal*, Vol. 13, No. 2, pp. 818-838.
- Ansari, A.A. and Alhussain, Z. (2019). The restricted five-body problem with cyclic kite configuration, *Journal of Dynamical Systems and Geometric Theories*, Vol. 17, No. 1, pp. 91-107. doi: 10.1080/1726037X.2018.1551720
- Ansari, A.A. and Kellil, R. (2019). Behavior of an infinitesimal-variable-mass body in CR3BP; the primaries are finite straight segments, *Punjab University Journal of Mathematics*, Vol. 51, No. 5, pp. 107-120.
- Ansari, A.A. and Prasad, S. (2018). The circular restricted three-body problem when both the primaries are heterogeneous spheroid of three layers and infinitesimal body varies its mass, *Journal Of Astrophysics and Astronomy*, Vol. 39, No. 57.
- Jeans, J.H. (1928). *Astronomy and Cosmogony*, Cambridge University Press, Cambridge.
- Kumari, R. and Kushvah, B.S. (2013). Equilibrium points and zero velocity surfaces in the restricted four-body problem with solar wind drag, *Astrophys Space Sci.*, Vol. 344, No. 2, pp.

- 347-359.
- Lichtenegger, H. (1984). The dynamics of bodies with variable masses, *Celest. Mech.*, Vol. 34, pp. 357-368.
- Lukyanov, L.G. (2009). On the restricted circular conservative three-body problem with variable masses, *Astronomy Letters*, Vol. 35, No. 5, pp. 349-359.
- Marchesin, M. and Vidal, C. (2013). Spatial restricted rhomboidal five-body problem and horizontal stability of its periodic solutions, *Celest Mech Dyn Astro.*, Vol. 115, pp. 261-279, doi:10.1007/s10569-012-9462-7
- Meshcherskii, I.V. (1949). *Works on the Mechanics of Bodies of Variable Mass*, GITTL, Moscow.
- Ollongren, A. (1988). On a particular restricted five-body problem: An analysis with computer algebra, *J. Symbolic computation*, Vol. 6, pp. 117-126.
- Pandey, L.P. and Ahmad, I. (2013). Periodic orbits and bifurcation in the Sitnikov four-body problem when all the primaries are oblate, *Astron Astrophys*, Vol. 345, pp. 73-83.
- Ragos, O., Papadakis, K.E. and Zagouras, C.G. (1997). Stability regions and quasi-periodic motion in the vicinity of triangular equilibrium points, *Celest Mech Dyn Astro.*, Vol. 67, No. 4, pp. 251-274.
- Shahbaz Ullah, M. and Hassan, M.R. (2014). Connection between three-body configuration and four-body configuration of the Sitnikov problem when one of the masses approaches to zero: circular case, *Astron. Astrophys*, Vol. 353, pp. 53-64.
- Shahbaz Ullah, M., Bhatnagar, K.B. and Hassan, M.R. (2014). Sitnikov problem in the cyclic kite configuration, *Astrophys Space Sci.*, Vol. 354, pp. 301-309.
- Shoaib, M., Kashif, A.R. and Csillik, I.S. (2017). On the planar central configurations of rhomboidal and triangular four-and five-body problems, *Astrophys Space Sci.*, Vol. 362, pp. 182.
- Shrivastava, A.K. and Ishwar, B. (1983). Equations of motion of the restricted problem of three bodies with variable mass, *Celest. Mech.*, Vol. 30, pp. 323-328.
- Singh, J. and Ishwar, B. (1984). Effect of perturbations on the location of equilibrium points in the restricted problem of three bodies with variable mass, *Celest. Mech*, Vol. 32, pp. 297-305.
- Singh, J. and Ishwar, B. (1985). Effect of perturbations on the stability of triangular points in the restricted problem of three bodies with variable mass, *Celest. Mech*, Vol. 35, pp. 201-207.
- Singh, J. (2003). Photogravitational restricted three-body problems with variable mass, *Indian Journal of Pure and Applied Math.*, Vol. 32, No. 2, pp. 335-341.
- Singh, J. and Leke, O. (2010). Stability of photogravitational restricted three-body problem with variable mass, *Astrophys. Space Sci.*, Vol. 326, No. 2, pp. 305-314.
- Singh, J. and Vincent, A.E. (2016). Out-of-plane equilibrium points in the photogravitational restricted four-body problem with oblateness, *British Journal of Mathematics and Computer Science*, Vol. 19, No. 5, pp. 1-15.
- Zhang, M.J., Zhao, C.Y. and Xiong, Y.Q. (2012). On the triangular libration points in photogravitational restricted three-body problem with variable mass, *Astrophys. Space Sci.*, Vol. 337, pp. 107-113. doi:10.1007/s10509-011-0821-8